PARAMETRIC SENSITIVITY OF A PARTIALLY EVAPORATING ORGANIC RANKINE CYCLE WITH THERMAL NON-EQUILIBRIUM EXPANSION

Xander van Heule[1]*, Michel De Paepe[1,2], Steven Lecompte[1,2]

[1] Department of Electromechanical, Systems and Metal Engineering, Ghent University, Sint-Pietersnieuwstraat 41, 9000 Ghent, Belgium
[2] FlandersMake@Ugent – Core lab EEDT-MP, www.flandersmake.be

*Corresponding Author: Xander.vanheule@ugent.be

ABSTRACT

Currently, a large share of the primary energy ends up as unused residual heat. This heat has a wide temperature range up to 200°C. Today, most high-temperature heat streams are already utilized but there is still large potential to utilize the low-temperature streams (<100°C). One method to utilize this heat is the application of heat-to-power cycles such as an organic Rankine cycle. However, these cycles are less effective when the heat stream has a lower temperature. Therefore, alternative cycles are proposed in literature. One cycle, promising for low-grade heat, is the trilateral flash cycle where the working fluid is heated in the evaporator to the point of saturated liquid. As such, the second law efficiency is increased due to the reduction of the exergy losses associated to a better temperature matching of the heat carrier and working fluid. However this cycle results in high mass flow rates and thus a high pump power. A solution is to partially evaporate into the two-phase liquid-vapour region. In this way, an optimum between temperature matching and the pump power can be found. Two-phase expansion is however complex and additional non-equilibrium phenomena are encountered. A modelling accounting for these effects was developed in a previous work. In this work, the impact of the expander dimensions, cut-off ratio, and evaporating temperature on the cycle performance will be elaborated. In this way, the sensitivity of the cycle in optimum conditions is studied as well as off-design operation for varying expander dimensions. Results show that a larger diameter resulted in higher power recovery, with a net power recovery of 491.23 W for a diameter of 0.11 m compared to 477.94 W at a diameter of 0.09 m.

1 INTRODUCTION

Minimizing the effects of global warming is currently one of the greatest tasks for humanity. This is achieved by reducing the emissions of greenhouse gasses, which can be achieved in a wide variety of ways. One approach is to increase energy efficiency. Currently, an estimated 52% of the global energy input is lost in the form of waste heat (Firth *et al.*, 2019) of which around 63% is low-temperature waste heat below 100°C (Forman *et al.*, 2016). There exist multiple technologies to reuse this heat in a meaningful way. One mature technology to utilize waste heat is the organic Rankine cycle (ORC) which transforms the waste heat into useful mechanical power. However, the performance of this technology reduces quickly with lower-temperature (<100°C) heat sources (Li *et al.*, 2017). Therefore, other alternative heat-to-power cycles are proposed that show increased effectiveness with low-temperature heat sources (Paanu *et al.*, 2012, Saghafifar *et al.*, 2019).
In this work, the focus is on the Trilateral Flash Cycle (TFC). This cycle seems identical to the basic ORC as can be seen from the layout in Figure 1. Where point 1 to 2 is the pump, point 2 to 3 the evaporator with point 6 the inlet of the heat source, point 3 to 4 the expander, and point 4 to 1 the condenser with point 7 the inlet of the heat sink. The difference between the basic ORC and the TFC can be seen in the Ts diagram in Figure 1. In the basic ORC, the outlet of the evaporator, or the inlet of

https://doi.org/10.52202/077185-0194

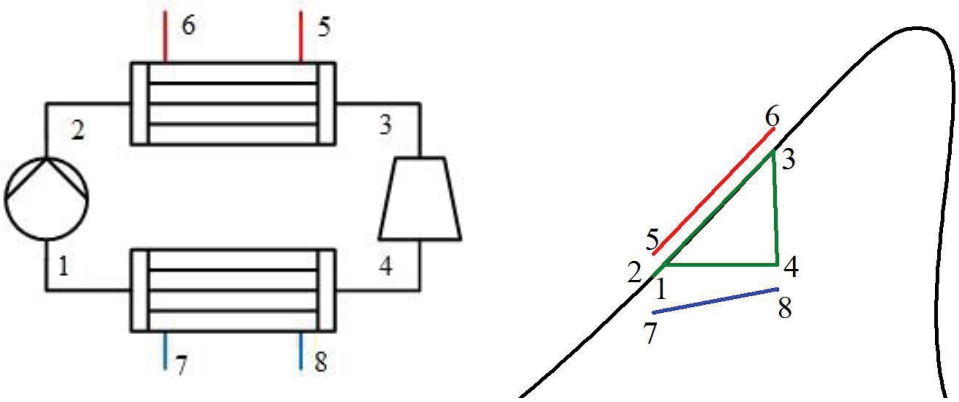

Figure 1: P&ID and TS diagram of a TFC.

the expansion machine, is within the superheated region while it is a saturated liquid for the TFC. Due to the omission of the phase change in the evaporator, the thermal efficiency is intrinsically lower compared to the basic ORC (Dipippo, 2007). However, the second law efficiency is higher than the ORC due to the improved temperature profile matching of the heat source with the working fluid (Lecompte *et al.*, 2015a). This is due to the reduction of the exergy destruction in the evaporator during constant temperature heat transfer while the working fluid evaporates. This higher net power output is especially prevalent at lower heat source temperatures (Woodland *et al.*, 2020). This cycle seems promising, but some problems arise. Firstly, there is currently a lack of suitable two-phase expanders with high enough adiabatic efficiencies, but studies have shown that this is possible (Paanu *et al.*, 2012). Secondly, the TLC requires large flow rates as the latent heat is omitted (Fischer, 2011). This can be resolved by partly evaporating the working fluid instead of working with a saturated liquid at the outlet of the evaporator. In this manner, the flow rate is drastically reduced and the net power of the cycle can be improved due to the reduced requirements of the pumping power (Lecompte *et al.*, 2013). This cycle is known as the partially evaporating organic Rankine cycle (PEORC).

When the TLC, PEORC, or other cycles which incorporate two-phase expansion are studied in literature, the expansion is modeled with certain assumptions. Often, a fixed isentropic efficiency is chosen. The other assumption frequently taken is that of thermodynamic equilibrium during the expansion process. This assumption has been shown not to always agree with experimental data. For Lysholm expanders operating under two-phase expansion, it was found to correlate relatively well with experiments (Öhman and Lundqvist, 2013) but not for reciprocating expanders (Kanno and Shikazono, 2015), where there were thermal non-equilibrium conditions measured during the expansion. The temperature of the liquid was determined to be greater than the saturation temperature corresponding to the instantaneous pressure. These observations were paired with non-equilibrium losses (Kanno and Shikazono, 2017). These losses could have an impact on the predictions of cycle performance which incorporate this type of expansion within its cycle.

In earlier work (van Heule *et al.*,2023), a model was constructed to predict the behavior of a two-phase expansion process with the inclusion of the possible thermal non-equilibrium states. This was achieved by the implementation of an adapted homogeneous relaxation model (HRM). The HRM adds a vapour generation rate equation to the homogeneous equilibrium model (HEM). With this additional equation, the mixture is no longer required to be in an equilibrium state. Instead, it can be the combination of a saturated vapour and a superheated liquid within the expansion chamber, as was experimentally determined by Kanno and Shikazono (2015). The vapour generation rate equation is based on a relaxation equation (Downar-Zapolski *et al.*, 1996) with a specific relaxation time. This relaxation time is in turn dependent on the expansion process. In this work, the expansion model is implemented within a PEORC with set boundary conditions. Secondly, the impact and sensitivity of the boundary conditions are investigated on the cycle performance. The investigated parameters are the expander dimensions and the influence of the heat source.

https://doi.org/10.52202/077185-0194

2 METHODS

2.1 Thermal non-equilibrium two-phase expansion

As mentioned in Section 1, the mixture within the expansion chamber could be within a non-equilibrium state when the expansion happens faster than the evaporation of liquid. As a result, the liquid is in a superheated state. This was chosen to be modeled with an adapted homogeneous relaxation model. This methodology extends the standard conservation equations with a vapour generation rate equation. This equation limits the evaporation rate that can occur through an empirical thermal relaxation time and is presented in equations (1) and (2).

$$\frac{\Gamma_g}{\rho} = -\frac{x-\bar{x}}{\Theta} \tag{1}$$

$$\Theta = \Theta_0 \cdot \epsilon^a \cdot \psi^b \tag{2}$$

where Γg is the volumetric vapour generation rate, ρ the mixture density, x the actual vapour quality, $\bar{x}$ the equilibrium vapour quality, Θ the relaxation time, ϵ the void fraction and ψ the non-dimensional pressure difference defined in equations (3) and (4) depending on the operational pressure.

$$\psi = \frac{p_s - p}{p_s} \quad if\ p < p_{lim} \tag{3}$$

$$\psi = \frac{p_s - p}{p_c - p_s} \quad if\ p > p_{lim} \tag{4}$$

where p_s is the saturation pressure corresponding to the liquid superheat, p is the actual pressure, p_c is the critical pressure, and p_{lim} an empirical pressure threshold. The values of the numerical parameters Θ_0, a, and b in equation (2), determined experimentally by Downar-Zapolski *et al.* (1996), are listed in Table 1.

Table 1: Net power of a PEORC for varying evaporating temperature and vapour quality.

	Θ_0	a	b
Equation (3) by Downar-Zapolski *et al.* (1996)	$6.51*10^{-4}s$	-0.257	-2.24
Equation (4) by Downar-Zapolski *et al.* (1996)	$3.84*10^{-7}s$	-0.54	-1.76
Equation (3) fitted to data of Kanno and Shikazono (2017)	$9*10^{-15}s$	-0.7	-15.7

The empirical pressure threshold was established to be 10 bar. These values were based on water flowing through a diverging nozzle. These values are dependent on the working fluid and the process conditions under which the expansion is taking place. Therefore, the relaxation model was adapted by van Heule *et al.* (2023) based on the data of Kanno and Shikazono (2017) as this was the best fitting available experimental data. It consists of water which is expanded within a cylindrical container with a free piston actuator. The superimposed movement profile by the researchers was a trapezoidal movement. The best fitting values for the numerical parameters Θ_0, a, and b in equation (2) based on the data of Kanno and Shikazono (2017) were determined to be $9*10^{-15}s$, -0.7 and -15.7 respectively as also presented in Table 1. These values are only valid for the dimensionless pressure given by the definition of equation (3) as there is no experimental data available above 10 bar. Here it was thus assumed that the threshold pressure is 10 bar.

The expansion model applies the conservation equations of mass and energy on the expansion chamber together with equations (1), (2), and (3) and the numerically determined values mentioned above to determine the thermodynamic state of the expanding fluid at each time step. This is achieved by keeping track of the mass and internal energy of each fluid state separately. The actual vapour quality can be determined via the mass ratio as depicted in equation (5), while the equilibrium vapour quality of the

https://doi.org/10.52202/077185-0194

current mixture can be determined based on the specific internal energy of the expansion chamber as depicted in equation (6).

$$x = \frac{m_g}{m_l + m_g} \tag{5}$$

$$\bar{x} = \frac{u - u_l}{u_g - u_l} \tag{6}$$

where m_g and m_l are respectively the amount of vapour and liquid mass present within the expansion chamber, u is the specific internal energy of the mixture, and u_g and u_l are the specific internal energy of the vapour and liquid phase respectively. Based on the density and specific internal energy of the vapour phase, the pressure of the expansion chamber can be determined. The liquid temperature is then determined through this pressure and the specific internal energy of the liquid phase through REFPROP 10 (Lemmon *et al.*, 2018). The saturation pressure corresponding to this liquid temperature is then used to determine the vapour generation rate in that instance of time. In this manner, the thermodynamic state of the expansion chamber is determined through time. The timestep is taken small enough so that a smaller time step does not alter the solution, but large enough to save on required calculation power.

2.2 Partial evaporating organic Rankine cycle

As explained in Section 1, the PEORC is an ORC where the evaporator does not fully evaporate the working fluid. In this work, one specific set of boundary conditions was chosen to study the impact of certain parameters on the performance of the PEORC. These boundary conditions are listed in Table 2. The listed expander diameter is the internal diameter of the reciprocating expander and the clearance length is the distance of the piston to the bottom of the expansion chamber. This is thus the height of the dead volume of the expansion chamber. Figure 2 presents an example of this cycle with a vapour quality of 0.3 at the evaporator outlet. Point 1 in this figure is determined by the condensing pressure and the subcooling before the pump as listed in Table 2. Point 2 is found by applying the isentropic pump efficiency between point 1 and the evaporating pressure. Point 3, at the inlet of the expander, is fixed by the choice of vapour quality. Point 4* is a representation of the thermodynamic state after the expansion stroke. This state is not necessarily in a stable condition as it could still consist of a superheated liquid and a saturated vapour. Therefore, point 4* is plotted on the diagram based on the density and specific internal energy of the mixture. Point 4 is the outlet of the expander. The process from point 4* to point 4 in Figure 2 is an isochoric process which thus includes both the over- or under-expansion losses and the non-equilibrium losses occurring when the expansion chamber comes in contact with the condenser. Finally, the condenser closes the cycle between points 4 and 1. Depending on the examined vapour quality at the evaporator outlet, the pinch point condition can occur at the saturated liquid point in the heat exchanger (point 5b), or the working fluid inlet side (point 6). The cycle model calculates both possibilities and applies the one that returns a valid temperature profile between the two heat exchange fluids. This also results in the calculation of the mass flow rate of the working fluid. In general, the pinch point condition only occurs at the working fluid inlet side for small vapour qualities at the expander inlet. The expander dimensions themselves are based on a reciprocating expander for waste heat recovery of a truck engine (Rijpkema *et al.*, 2021). Both the intake and expansion stroke happen during one piston movement. The ratio of the inlet stroke to the entire stroke is assumed equal to 25% as this is a common ratio for the cut-off ratio (Glavatskaya *et al.*, 2012). The rotational speed and stroke length of the expander are a result of the movement of the free piston and the matching of the required working fluid mass flow rate which was previously determined in the evaporator calculation. Lastly, the chosen working fluid is R1233ZD(E) as it has good matching fluid properties for this type of cycle, as Bianchi et al. (2017) studied.

https://doi.org/10.52202/077185-0194

Table 2: Boundary conditions of the applied PEORC.

Evaporating temperature	100 °C
Condensing temperature	20 °C
Working fluid	R1233ZD(E)
Heat source fluid	Air
Heat source temperature	110 °C
Heat source mass flow rate	0.2 kg/s
Subcooling pump	5 °C
Evaporator pinch point	5 °C
Pump isentropic efficiency	70 %
Expander diameter	0.09 m
Expander clearance length	0.003 m
Cut-off ratio	25 %

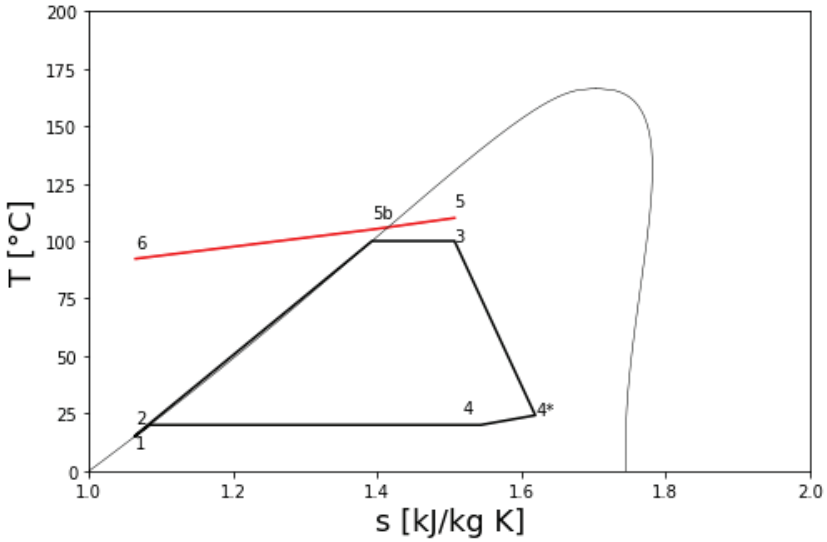

Figure 2: Example TS diagram of a PEORC with an expander vapour quality of 0.3.

In the following section, cycles with different vapour qualities will be compared. This will mostly occur based on the net power of the cycles as defined in equations (7), (8), and (9).

$$W_{exp} = \frac{\int p \cdot dV}{t_{cycle}} \tag{7}$$

$$W_{pump} = \dot{m}_{wf} \cdot (h_2 - h_1) \tag{8}$$

$$W_{net} = W_{exp} - W_{pump} \tag{9}$$

where W_{exp} is the power obtained in the expander, W_{pump} the power required for the pump, W_{net} the net power obtained from the cycle, p the instantaneous pressure within the expansion chamber, V the volume of the expansion chamber, t_{cycle} the time required for the piston to complete a cycle, $\dot{m}_{wf}$ the mass flow rate of the working fluid, h_1 and h_2 the specific enthalpy corresponding to the pump inlet and outlet respectively as illustrated on Figure 2. The net power is used as a comparison because it is directly linked to the second law efficiency presented in equation (10) (Lecompte *et al.*, 2015b).

$$\eta_{II} = \frac{W_{net}}{E_{hs,in}} \tag{10}$$

https://doi.org/10.52202/077185-0194

$$E_{hs,in} = \dot{m}_{hs} \cdot (h_5 - h_0 - T_0 \cdot (s_5 - s_0)) \quad (11)$$

where η_{II} is the second law efficiency and $E_{hs,in}$ is the exergy flow of the heat source at the inlet, this corresponds to point 5 in Figure 2, as defined in equation (11). Where $\dot{m}_{hs}$ is the mass flow rate of the heat source, h_5 and s_5 are the specific enthalpy and specific entropy of point 5 respectively. Lastly h_0, s_0, and T_0 are the conditions of the dead state. The dead state is typically chosen as either the inlet conditions of the cooling fluid or ambient conditions. In this work, the ambient condition is chosen as the dead state which corresponds to a pressure of 1 bar and a temperature of 20 °C. When comparing cycles with different vapour qualities at the expander inlet, the second law efficiency and the net power are linearly dependent because the inlet conditions of the heat sources are kept constant. Therefore, as long as the sensitivity of the heat source inlet conditions is not tested, it is possible to compare the net power values instead of the second law efficiencies.

3 RESULTS

Firstly, the optimum net power is heavily dependent on the mass flow rate as this has a linear impact on the pumping power through equation (8). While the mass flow rate is heavily impacted by the choice of vapour quality at the expander inlet as was elaborated in literature and is presented in Figure 3 for the specific case studied in this work. As can be seen in the figure, low vapour qualities require exponentially higher pumping powers. As a result, the optimum vapour quality for the boundary conditions listed in Table 2 is found to be 0.51 with a net power of 477.94 W as also shown in Figure 4. This corresponds with a second law efficiency of 20.5%, which is within a realistic region (Lecompte *et al.*, 2015b). For higher vapour qualities, the heat transfer in the evaporator becomes limiting due to the pinch point condition in the evaporator which in turn limits the net power of the cycle. Additionally, the found rotational speed for the expander becomes drastically low for the low flow rates. Therefore, the sudden drop-off in Figure 4 is also a result of the expander dimensions where the solver doesn't find a solution for the cycle.

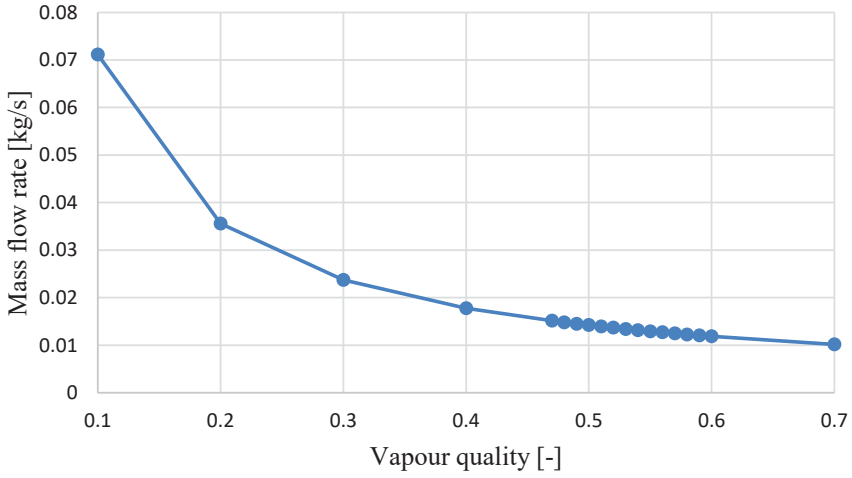

Figure 3: Mass flow rate of the working fluid of a PEORC with the boundary conditions of Table 2 in function of vapour quality.

https://doi.org/10.52202/077185-0194

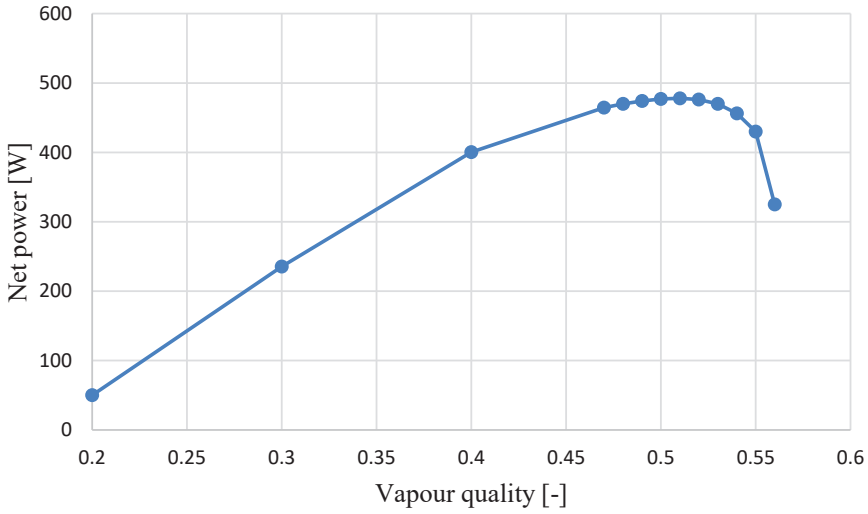

Figure 4: Net power produced of a PEORC with the boundary conditions of Table 2 in function of vapour quality.

3.1 Sensitivity of the expander dimensions

The rotational speed of the expander at the found optimum corresponds well with the operational point of the cycle on which the expander dimensions are based (Rijpkema *et al.*, 2021). This leads to reason that the expander dimensioning itself could have a significant impact on the operation of a PEORC running on a fixed heat source. Therefore, the expander diameter, expander clearance length, and cut-off ratio will be varied to a larger and smaller value while the impact on the PEORC is investigated. Figure 5 presents the net power in function of the vapour quality for three different expander diameters and Figure 6 presents the net power in function of the vapour fraction for three different initial clearance lengths of the expander. All other parameters remain identical to the ones listed in Table 2 for both figures.

The expander diameter has a relatively large impact on the optimum vapour quality with a lower optimum vapour quality for a larger diameter. This is likely a result of a larger volume, which results in more evaporation in the cylinder for a similar volumetric vapour generation rate. Additionally, the maximum net power of the cycle also increases with a value of 491.23 W. This seems like a small increase, but the required pumping power is also larger due to the lower vapour quality which means the power harvested in the expander was increased more. This implies that an optimized expander, including the non-equilibrium effects, is an important part of designing a PEORC. Lastly, the possible operating range is influenced by the expander sizing. As mentioned before, the sudden drop in Figure 4 corresponds to cycles for which the solver can't find a solution due to the very low expander rotational speed. For the larger bore diameter, this point is further away from the optimum vapour quality while for the lower diameter, it falls almost immediately after the optimum vapour quality. In a realistic operational scenario, it would be safer to use the more stable design (i.e. larger diameter) as the working point will change if the heat source isn't constant.

A similar effect is observed for a variation of the initial clearance length with regard to the optimum vapour quality, where a greater clearance length results in lower optimum vapour qualities. However, the resulting maximum net power is lower. This indicates that an overall larger volume, due to the increased dead volume, does not necessarily indicate a higher net power as was the case for the larger diameter. This would be a result of the larger dead volume, leading to larger re-expansion losses.

https://doi.org/10.52202/077185-0194

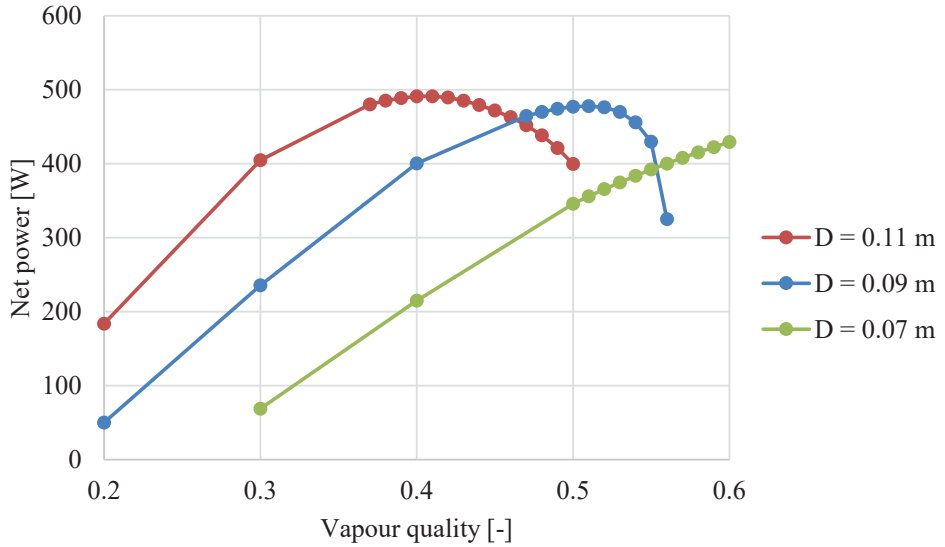

Figure 5: Net power produced of a PEORC with the boundary conditions of Table 2 in function of vapour quality for three different expander diameters.

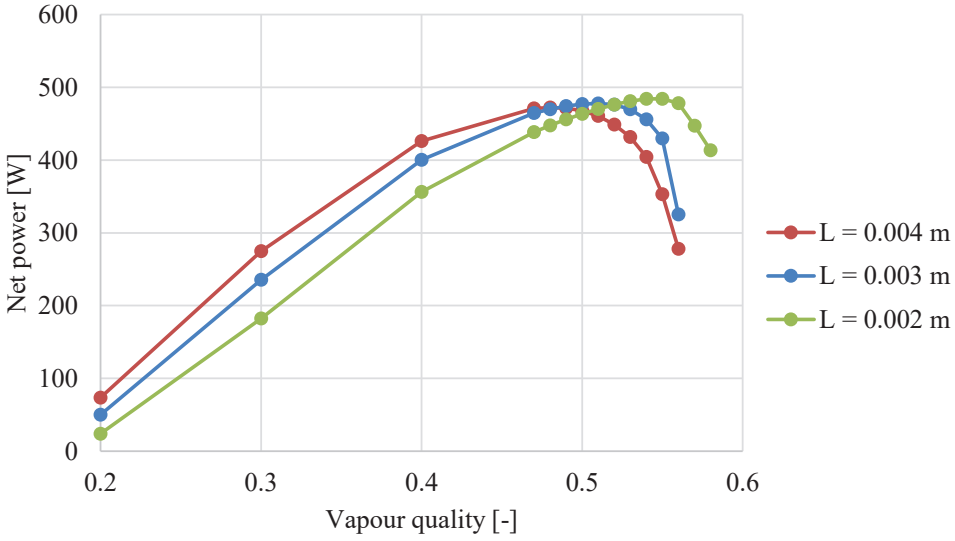

Figure 6: Net power produced of a PEORC with the boundary conditions of Table 2 in function of vapour quality for three different initial clearance lengths.

Lastly, the effect of the cut-off ratio, the ratio between the durations of the intake stroke and the intake and expansion strokes combined, is examined with a higher and lower value as listed in Table 2, this is presented in Figure 7. The optimum vapour quality is lower for higher cut-off ratios, meaning that the intake stroke is a larger part of the entire stroke. This implies that more mass can enter the expansion chamber during each stroke resulting in a higher possible mass flow rate for the same expander speed. The optimum vapour quality for the three different cut-off ratios occur for around the same expander cycle speed. Therefore, the cut-off ratio has no impact on the expander speed for the optimum vapour quality. However, the stability is drastically reduced with high cut-off ratios as the drop where no solutions are found happens soon after the optimum point but the maximum net power is drastically higher.

https://doi.org/10.52202/077185-0194

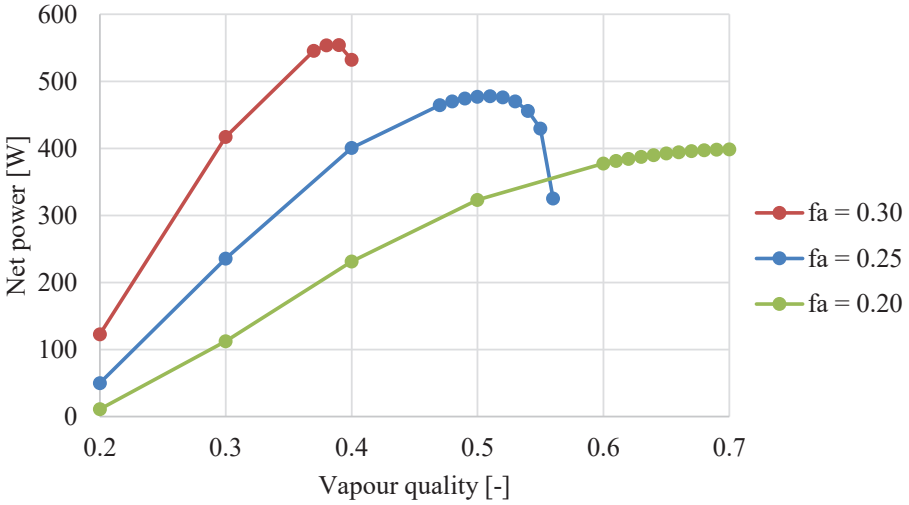

Figure 7: Net power produced of a PEORC with the boundary conditions of Table 2 in function of vapour quality for three different cut-off ratios.

Table 3: Optimum vapour qualities for different evaporating temperatures.

Evaporating temperature [K]	Optimum vapour quality [-]	Net power [W]
372.15	0.71	468.65
372.65	0.60	471.87
373.15	0.51	477.94
373.65	0.42	486.90
374.15	0.34	499.08
374.65	0.27	515.35

Table 4: Net power of a PEORC for varying evaporating temperature and vapour quality.

$W_{net}[W]$	Vapour quality [-]									
T [K]	0.45	0.46	0.47	0.48	0.49	0.50	0.51	0.52	0.53	0.54
373.10	443.8	451.7	458.8	464.9	470.0	473.9	476.5	477.2	475.2	469.0
373.11	445.2	453.0	459.9	465.9	470.9	474.6	476.9	477.2	474.6	467.2
373.12	446.6	454.3	461.1	467.0	471.8	475.3	477.3	476.5	473.8	465.0
373.13	448.0	455.6	462.3	468.0	472.6	475.9	477.6	476.9	472.7	462.4
373.14	449.3	456.8	463.4	469.0	473.4	476.5	477.8	476.6	471.5	459.4
373.15	450.7	458.1	464.5	470.0	474.2	477.0	477.9	476.1	470.0	456.0
373.16	452.0	459.3	465.6	470.9	475.0	477.5	478.0	475.5	468.2	/
373.17	453.3	460.5	466.7	471.8	475.7	477.9	478.0	474.8	466.0	/
373.18	454.6	461.7	467.8	472.7	476.3	478.2	477.8	473.8	463.4	/
373.19	455.9	462.9	468.8	473.6	476.9	478.5	477.5	472.6	460.3	/
373.20	457.2	464.1	469.8	474.4	477.5	478.7	477.1	471.1	456.9	/

3.2 Impact of the evaporating temperature

The impact of the chosen high-pressure level is investigated next. The found vapour quality optimum is quite sensitive to the evaporation pressure. For example, setting the evaporating saturation temperature one degree lower, to 99 °C, already gives a new optimum vapour quality of 0.71 with a net power recuperation of 468.65 W. Other examples are listed in Table 4. Therefore, the impact of the evaporating temperature will be largely investigated on a narrow range of temperatures and vapour

https://doi.org/10.52202/077185-0194

qualities. A subset of these are listed in Table 4, but the conclusions drawn here are valid for the entire tested domain. The optimum value for each temperature level in Table 4 is shaded green.
It is observed that the optimum point shifts to higher vapour qualities when the saturation temperature decreases. This can be a result of the pinch point condition because a lower evaporation temperature results in higher required mass flow rates at the same vapour quality, which increases the required pumping power. This is likely offset by a higher vapour quality as was discussed in Figure 3, which likely also shifts the optimum point here for lower evaporating temperatures.

Secondly, it is also observed that the maximum net power recovery goes up with the evaporating temperature. This is according to literature, where it has been shown that the TLC has a second law efficiency which is higher than the ORC. However, this would, according to literature, have a limit. For the chosen boundary conditions, the simulation also starts to find no valid solution for vapour qualities slightly higher than the optimum, similar to what can be seen in previous figures. This edge of stability also shifts to lower vapour qualities for higher evaporating temperatures. This can also impact the optimum result if the optimum falls in the unstable zone. This actual optimum is found around an evaporating temperature of 375.98 K or 102.83 °C with a net power recovery of 593.43 W. However, the instability is indeed very close to the corresponding optimum vapour quality of 0.13 which could give rise to problems for unsteady heat sources.

3.3 Impact of the heat source mass flow rate

Lastly, the mass flow rate of the heat source is varied. The constant mass flow rate of 0.2 kg/s in Table 2 is altered to both 0.1 and 0.3 kg/s. This change in mass flow rate drastically changes the required working fluid mass flow rate and thus the pumping power. The low heat source mass flow rate of 0.1 kg/s results in an optimum vapour quality of 0.16 which corresponds to a net power recovery of 506.83 W. The high mass flow rate of 0.3 kg/s results in an optimum vapour quality of 0.93 corresponding to a net power recovery of 478.73 W. However, because the heat source mass flow rate is varied, the second law efficiencies should be compared. These are 43.6 % and 14.0 % for the lower and higher heat source mass flow rates respectively while the standard case with a heat source mass flow rate of 0.2 kg/s has an optimum second law efficiency of 20.6 %. This indicates that the lower heat source mass flow rate is better at recovering the exergy within the waste heat stream for the given expander design parameters.

4 CONCLUSIONS

In this work, the sensitivity of a partially evaporating organic Rankine cycle towards the sizing of a piston expander is investigated. Compared to previous studies, this model also takes the thermal non-equilibrium effects within the expander into account and this based on an adapted homogeneous relaxation model. The studied parameters are the design parameters of the expander, the chosen evaporating temperature, and the mass flow rate of the heat source. Firstly, a higher heat source mass flow rate results in a more stable cycle but for a lower second law efficiency. Secondly, the chosen geometry of the expander has a big influence on the cycle. Both on the stability and on the vapour quality where the highest second law efficiency is achieved for bigger expander diameters with a value of 21.1 % for a diameter of 0.11 m compared to 20.6 % for a diameter of 0.09 m. A smaller expansion volume corresponds to a higher vapour quality where the optimum second law efficiency is achieved, with the optimum for a diameter of 0.11 m located at a vapour quality of 0.41 while for a diameter of 0.09 m it is found at 0.51. The cut-off ratio, the ratio between the intake and full stroke, also has a significant impact on the second law efficiency. Where higher cut-off ratios result in higher values, 23.9% for a cut-off ratio of 0.3 compared to 20.6% for a cut-off ratio of 0.25, but for a less stable cycle when fluctuations occur. Lastly, the evaporating temperature also impacts the cycle performance. A higher evaporating temperature results in lower optimal vapour qualities which is likely due to the changing required mass flow rate of the working fluid. The recovered net power also increases for higher evaporating temperatures.

https://doi.org/10.52202/077185-0194

NOMENCLATURE

Γ	volumetric vapour generation rate	(kg/m³s)
Θ	relaxation time	(s)
ρ	density	(kg/m³)
ϵ	void fraction	(-)
ψ	dimensionless pressure	(-)
E	exergy flow	(W)
h	specific enthalpy	(J/kg)
m	mass	(kg)
$\dot{m}$	mass flow rate	(kg/s)
p	pressure	(Pa)
s	specific entropy	(J/kgK)
t	time	(s)
u	specific internal energy	(J/kg)
V	volume	(m³)
W	power	(W)
x	vapour quality	(-)
$\bar{x}$	equilibrium vapour quality	(-)

Subscript

c	critical
cycle	cycle
exp	expander
g	gas/vapour
hs	heat source
II	second law
in	inlet
net	netto
l	liquid
pump	pump
s	saturation
wf	working fluid

REFERENCES

Bianchi, G., McGinty, R., Oliver, D., Brightman, D., Zaher, O., Tassou, S.A., Miller, J., Jouhara, H., 2017, Development and analysis of a packaged Trilateral Flash Cycle system for low grade heat to power conversion applications, *Thermal science and engineering progress,* vol. 4, no. 1: p. 113-121.

Dipippo, R., 2007, Ideal thermal efficiency for geothermal binary plants, *Geothermics*, vol. 36, no. 1: p. 276-285.

Downar-Zapolski, P., Bilicki, Z., Bolle, L., Franco, J., 1996, The non-equilibrium relaxation model for one-dimensional flashing liquid flow, *Int. J. Multiph. Flow*, vol. 22, no. 3: p. 473-483.

Firth, A., Zhang, B., Yang, A., 2019, Quantification of global waste heat and its environmental effects, *Appl. Energy,* vol. 235, no. 1: p. 1314-1334.

Fischer, J., 2011, Comparison of trilateral cycles and organic Rankine cycles, *Energy,* vol. 36, no. 1: p. 6208-6219.

Forman, C., Muritala, I.K., Pardemann, R., Meyer, B., 2016, Estimating the global waste heat potential, *Renewable Sustainable Energy Rev.,* vol. 57, no. 1: p. 1568-1579.

Glavatskaya, Y., Podevin, P., Lemort, V., Shonda, O., Descombes, G., 2012, Reciprocating expander for an exhaust heat recovery rankine cycle for a passenger car application, *energies*, vol. 5: p. 1751-1765.

https://doi.org/10.52202/077185-0194

Kanno, H., Shikazono, N., 2015, Experimental and modeling study on adiabatic two-phase expansion in a cylinder, *Int. J. Heat Mass Transf.*, vol 86, no. 1: p. 755-763.
Kanno, H., Shikazono, N., 2017, Modeling study on two-phase adiabatic expansion in a reciprocating expander, *Int. J. Heat Mass Transf.*, vol 104, no. 1: p. 142-148.
Lecompte, S., van den Broek, M., De Paepe, M., 2013, Thermodynamic analysis of the partially evaporating trilateral cycle, *Int. Seminar on ORC power systems,* p. 1-4.
Lecompte, S., Huisseune, H., van den Broek, M., Vanslambrouck, B., De Paepe, M., 2015a, Review of organic Rankine cycle (ORC) architectures for waste heat recovery, *Renewable and sustainable energy reviews*, vol. 47, no. 1: p. 448-461.
Lecompte, S., Huisseune, H., van den Broek, M., De Paepe, M., 2015b, Methodical thermodynamic analysis and regression models of organic rankine cycle architectures for waste heat recovery, *Energy,* vol. 87, no. 1: p. 60-76.
Lemmon, E.W., Bell, I.H., Huber, M.L., McLinden, M.O., 2018, NIST Standard Reference Database 23: Reference Fluid Thermodynamic and Transport Properties-REFPROP, Version 10.0, *National Institute of Standards and Technology*, Standard Reference Data Program, Gaithersburg.
Li, Z., Huang, Y., Qian, G., Chen, F., Yu, X., Roskilly, A., 2017, Comparison of Trilateral Rankine Cycle, Organic Flash Cycle and basic Organic Rankine Cycle for low grade heat recovery, *9th international conference on applied energy*, Energy Procedia 142: p. 1441-1447.
Öhman, H., Lundqvist, P., 2013, Experimental investigation of a lysholm turbine operating with superheated, saturated and 2-phase inlet conditions, *Appl. Therm. Eng.*, vol. 50, no. 1: p. 1211-1218.
Paanu, T., Niemi, S., Rantanen, P., 2012, Waste heat recovery – bottoming cycle alternatives, *Proc of the university of Vaasa*, vol. 175: p. 1-26.
Rijpkema, J., Thantla, S., Fridh, J., Andersson, S.B., Munch, K., 2021, Experimental investigation and modeling of a reciprocating piston expander for waste heat recovery from a truck engine, *Appl. Therm. Eng.,* vol 186, no. 1: p. 1-15.
Saghafifar, M., Omar, A., Mohammadi, K., Alashkar, A., Gadalla, M., 2019, A review of unconventional bottoming cycles for waste heat recovery: Part I – Analysis, design, and optimization, *Energy conversion and Management*, vol. 198, no. 1: p. 110905.
van Heule, X., Skiadopoulos, A., Manolakos, D., De Paepe, M., Lecompte, S., 2023, Modelling of two-phase expansion in a reciprocating expander, *Appl. Therm. Eng.*, vol. 218, no. 1: p. 1-10.
Woodland, B.J., Ziviani, D., Braun, J.E., Groll, E.A., 2020, Considerations on alternative organic Rankine Cycle congurations for low-grade waste heat recovery, *Energy*, vol. 193, no. 1: p. 1-17.

ACKNOWLEDGEMENT

I would like to thank the Research Foundation-Flanders for their financial support through FWO-Flanders grants (1SD9723N).

https://doi.org/10.52202/077185-0194